Journal of
Ship&Ocean
Technology
©DECEMBER 2008

SOTECH Vol. 12, No. 4, pp. 20 ~ 31, 2008

Rudder Gap Cavitation Suppression Using Gap Flow Blocking Devices

Jungkeun Oh[1], Changmin Lee[2], Hee Bum Lee[2], Shin Hyung Rhee[2], Jung-Chun Suh[2] and Hyochul Kim[1]

[1] Jungseok Research Institute of International Logistics and Trade, Inha University, Incheon, Korea
[2] Department of Naval Architecture & Ocean Engineering, Seoul National University, Seoul, Korea;
Corresponding Author: o95414@snu.ac.kr

Abstract

Development of rudder gap flow blocking device for lift augmentation and cavitation suppression is presented. In order to verify the performance of this device, cavitation visualization and surface pressure measurements were carried out in a cavitation tunnel. Numerical simulations were conducted using a computational fluid dynamics code for more rigorous verification. The new rudder system is equipped with cam devices, which effectively close the gap between the horn/pintle and movable wing parts. The experimental and computational results show that the proposed rudder system is superior to the conventional rudder systems in terms of the lift augmentation and cavitation suppression.

Keywords: rudder cap cavitation, cavitation tunnel, gap flow blocking device

1 Introduction

Nowadays, the cavitation of the rudder system is frequently observed because cargo ships, such as container ships, are bigger and faster. Damages on the rudder system due to the cavitation are mostly seen around the leading edge and the gap region between the horn/pintle and movable wing parts, e.g., see Figure 1.

There have been several interesting studies on the suppression of this rudder cavitation with modified rudder shapes and/or various types of devices attached to the region inside or around the gap (Shen et al., 1997; Boo et al., 2003a, Boo et al., 2003b, Song et al., 2004, Kim et al., 2006, Choi and Chung, 2007, Park et al., 2007, Paik et al., 2008). However, many of them lack completeness in terms of suppressing the rudder cavitation and do not consider the additional devices to increase the rudder performance.

In the present study, a newly devised rudder system, which is recently proposed by the authors, is analyzed with regard to the lift augmentation and cavitation suppression. The new rudder system differs from conventional ones in the cam devices, which effectively close the gap between the horn/pintle and movable wing parts. Results from both model tests and numerical simulations using a computational fluid dynamics (CFD) code are

presented. Two types of model tests are carried out: one is visualization of the cavitation and; the other is surface pressure measurement in a cavitation tunnel at Seoul National University in Korea. For cavitation visualization, the pressure in the cavitation tunnel was decreased artificially to lower the cavitation number. The cavitation phenomenon was then recorded with a video camera and analyzed. For surface pressure measurements, holes were made on the surface of the model and the pressure was measured using a pressure transducer and scanivalve. The selected CFD code solves the Reynolds-averaged Navier-Stokes equations and was validated against existing experimental data (Rhee and Kim, 2006).

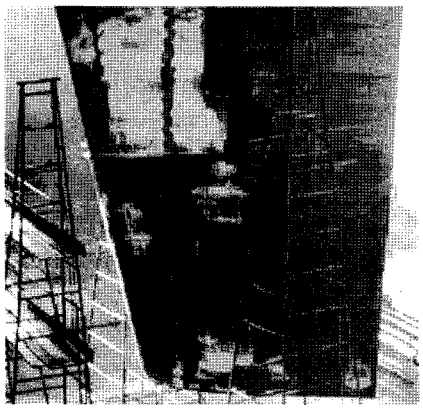

Figure 1: Erosion caused by rudder cavitation

2 Cononceptual design

The main difference of the new rudder system from the conventional ones is found near the gap between the horn/pintle and movable wing parts. Two types of cam devices are placed in the gap to block the flow through the gap. By blocking this flow, (1) the pressure difference on the sides of stationary part increases, which results in the lift augmentation, and (2) the negative pressure peaks are removed or mitigated, which eventually results in cavitation suppression. Figure 2 displays the conventional and new rudder systems with deflection angle of 5°.

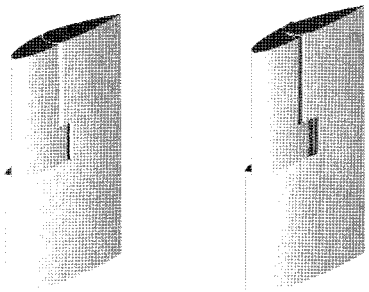

Figure 2: Three-dimensional views of rudder system: conventional (left) and new (right)

For the present study, two models (horn section shown in Figure 3 and pintle section shown in Figure 4) were designed and manufactured for two-dimensional (2D) experiments. In the present paper, only the results of the pintle section model with 5-degree deflection angle are presented.

Figure 3: 2D model shape for horn section

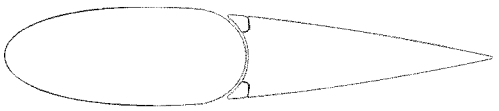

Figure 4: 2D model shape for pintle section

3 Experimental setup and method

Symmetrically shaped rudders are often used in common ships. In the present study, NACA0020 section was selected, which is similar to a typical rudder section. The models of the horn section and pintle section were made separately of aluminum alloy. The chord length of the whole section is 0.2m and the span length is 0.15m. Between the horn/pintle and movable part, the cam devices for blocking gap flow are inserted as shown in Figure 5.

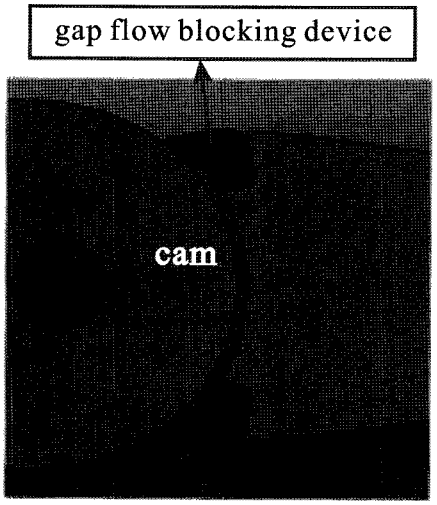

Figure 5: Gap flow blocking device for horn section

Figure 6 shows the models for cavitation visuali-zation (left) and surface pressure measure-ments (right). Each model was fixed to a circular end plate and the angle of attack is adjusted by simply rotating the end plate. There are 39 holes on the surface of the model to measure the surface pressure. The hole locations were determined carefully in such a way the there exists no interference between holes. The holes were located around mid-span with a 3mm interval, along a line that makes approximately five degrees with the flow direction. The diameter of

each hole is 2mm (see Figure 7)

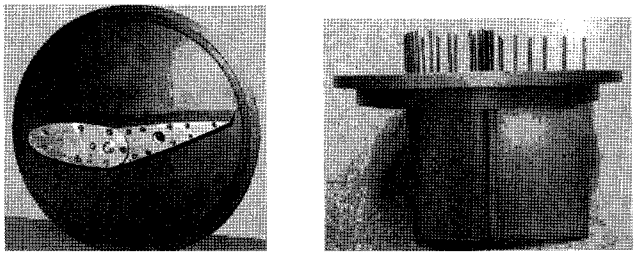

Figure 6: Test models for cavitation visualization (left) and surface pressure measurements (right)

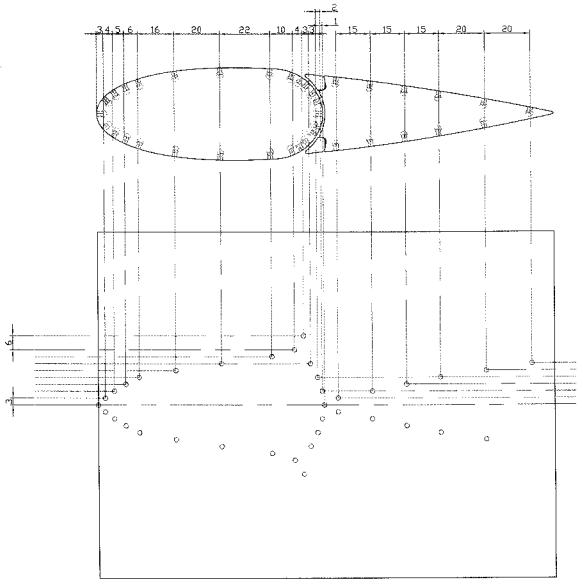

Figure 7: Pressure hole locations on pintle section

Model tests were carried out in the cavitation tunnel, whose measurement section extends 1 m long, 0.15 m wide, and 0.5 m high. The controllable pressure range is 15 kPa to 300 kPa and the maximum flow speed is 16 m/s.

4 Computational method

The computational results were obtained by solving the Reynolds-averaged Navier-Stokes (RANS) equations.

$$\frac{\partial \rho}{\partial t} + \nabla \cdot \left(\rho \vec{v} \right) = 0 \tag{1}$$

$$\frac{\partial}{\partial t}\left(\rho \vec{v} \right) + \nabla \cdot \left(\rho \vec{v} \vec{v} \right) = -\nabla p + \nabla \cdot \left(\bar{\bar{\tau}} \right) \tag{2}$$

where $\vec{v}$ is the velocity vector in the Cartesian coordinate system, p the static pressure, and τ the stress tensor.

The CFD code, FLUENT 6.2, employs a cell-centered finite-volume method. Convective terms are discretized using the second order accurate upwind scheme, while diffusive terms are discretized using the second order accurate central differencing scheme. The velocity-pressure coupling and overall solution procedure are based on a SIMPLEC type segregated algorithm. The convergence criteria in the present study were at least three orders of magnitude drop in the mass conservation imbalance and momentum equation residuals, which are deemed sufficient for most steady flow solutions.

Once the Reynolds averaging approach for turbulence modeling is applied, the Reynolds stresses resulting from the process must be modeled to close Equation (2). The so-called realizable k-ε turbulence model (Shih et al., 1995), which is based on the Boussinesq hypothesis with transport equations for the turbulent kinetic energy, k, and its dissipation rate, ε, was used for turbulence closure. The turbulent viscosity μ_t was computed by combining k and ε as $\mu_t = \rho C_\mu k^2/\varepsilon$, where C_μ is a function of the mean strain and rotation rates, the angular velocity of the system rotation, and k and ε. The realizable k-ε model is a variation of the standard k-ε model and has shown good performance for flows with strong streamline curvature, vortices, and rotation (Kim and Rhee, 2002; Rhee et al., 2005; Rhee and Makarov, 2005). For wall boundary conditions, the wall function approach based on the law of the wall was applied.

5 Results and discussion

To confirm that the gap flow blocking devices function as expected, cavitation inception tests and surface pressure measurements were carried out with the pintle section model with 5-degree deflection angle. The experimental condition is summarized in
Table 1.

Figure 8 is a schematic diagram of the experiments in the cavitation tunnel with a pressure transducer and scanivalve installed.

In the present study, the cavitation number (σ) and pressure coefficient are defined as:

$$S = \frac{P_{in} - P_v - P_d}{\frac{1}{2} r V_{in}^2} \tag{3}$$

$$-C_P = \frac{P_{in} - P_{foil}}{\frac{1}{2} r V_{in}^2} \tag{4}$$

P_d: Decompressed pressure in the cavitation tunnel

P_{in}: Pressure of the flow heading on the model

P_v: *Vapor pressure*

P_{foil}: *Surface pressure of each pressure hole of the model*

V_{in}: *Inflow velocity*

r : *Water density*

Table 1: Experimental condition

Model section	Reynolds No. (flow velocity)	Deflection angle (degrees)
Pintle	1.4×10^6 (7 m/s)	5

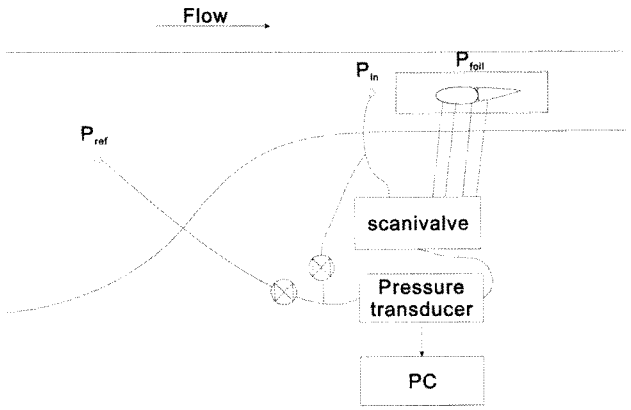

Figure 8: Schematic diagram of experiment

In the experiments, the cavitation inception is checked in the following way. First, the model is set in the tunnel with deflection angle of five degrees. The movable wing part is rotated in the counter-clockwise direction, so the visualization can be done through the bottom window of the test section. The flow speed is set to constant 7 m/s. While gradually depressurizing the tunnel, careful observation is made on the foil surface. Once the cavity is observed, put a hold on the depressurization and record the cavitation behavior using a video camera.

In the computations, the possible cavitation locations are identified first with the atmospheric pressure condition. Then further computations are carried out with decreasing reference pressure, and the negative C_p values at the possible cavitation locations are compared with the corresponding s at the given reference pressure. When the negative C_p values reach s, the incipient cavitation number is identified as s.

Table 2: Cavitation inception test results

Position	Incipient cavitation number			
	Open gap		Closed gap	
	Experiment	CFD	Experiment	CFD
0.467C	1.45	1.457		
0.4C		1.175	1.33	1.33
0.1C	1.15	0.992	1.25	1.109

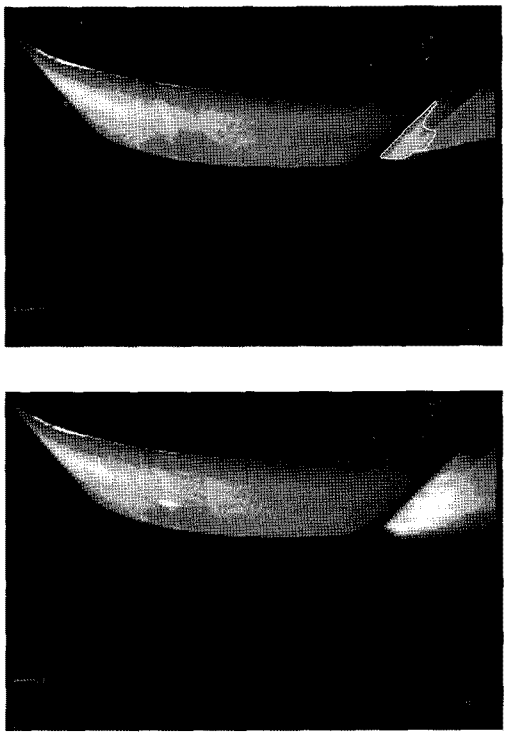

Figure 9: Incipient cavitation number and location (open gap):
$S = 1.45$ @ 0.467C (upper)
and $S = 1.15$ @ 0.1C (lower)

The incipient cavitation numbers identified by experiments and computations are listed in

Table 2. The corresponding images are shown in Figure 9 (open gap) and Figure 10 (closed gap). When the gap is open, cavitation is observed after the gap (0.467C) at s = 1.45. On the other hand, when the gap is closed, cavitation is observed before the gap (0.4C) at a lower s = 1.33. The same behavior is also confirmed by computations. From this observation, it is clear that by closing the gap, the cavitation is delayed and the damage on the movable wing part after the gap can be avoided or reduced. With further depressuri-zation, the leading edge (0.1C) cavitation is also observed. This leading edge cavitation occurs earlier when the gap is closed, because the whole rudder section with closed gap functions as a single hydrofoil and thus the suction side pressure decreases further than with open gap. Note that, with open gap, the flow between the gap results in less negative pressure on the suction side of this two-part rudder section. The discrepancy between experiments and computations at 0.4C (open gap) and 0.1C is attributed to the surface roughness that is not taken into account in computations.

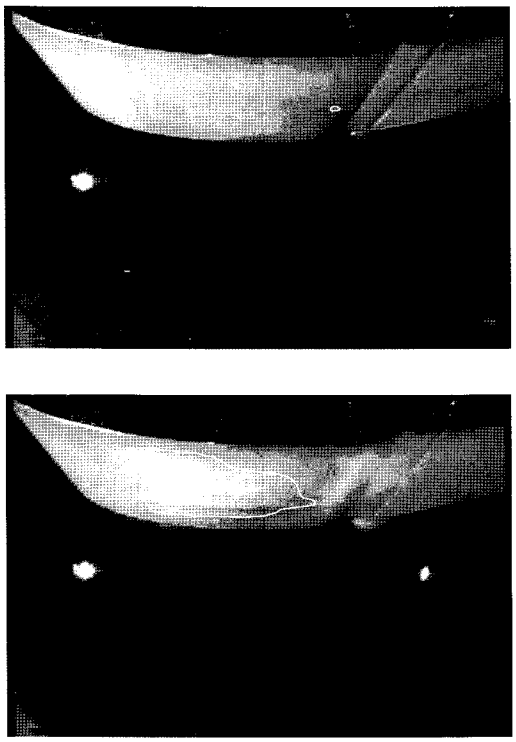

Figure 10: Incipient cavitation number and location (closed gap):
S = 1.33 @ 0.4C (upper)
and S = 1.25 @ 0.1C (lower)

In order to further investigate the effectiveness of the gap blocking devices, the surface pressure measurements were carried out at non-cavitating atmospheric conditions. Note that, due to the cavitation bubbles floating around and sucked into the pressure tap, the pressure measurements were not possible when the tank was depressurized.

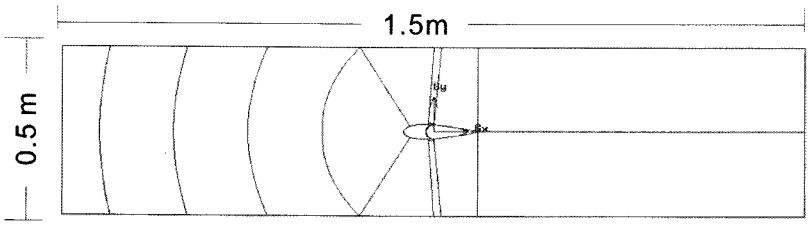

Figure 11: Computational domain

For corresponding computations, the domain extent was set to match the test section dimensions of the cavitation tunnel, except in the flow direction to ensure the proper inflow and outflow boundary conditions. Figure 11 and Figure 12 show the computational domain and grids, respectively. The computational conditions are same as the experiments.

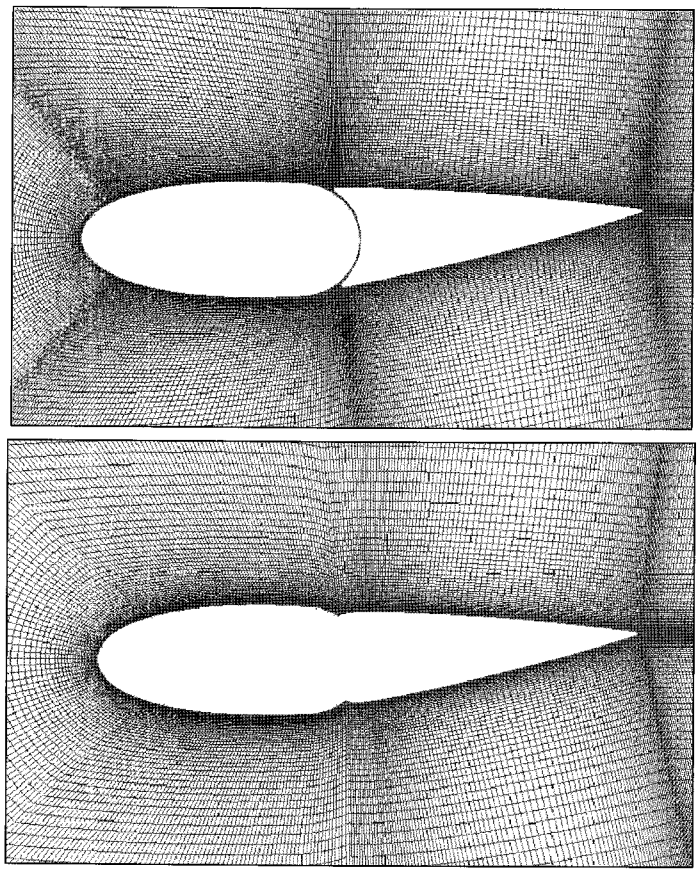

Figure 12: Computational grids: open gap (left), closed gap (right)

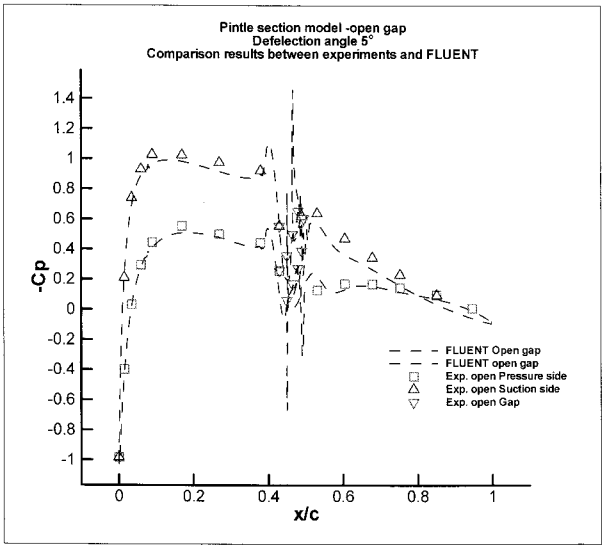

Figure 13: Surface pressure coefficient with open gap: Experiments (symbols); Computations (lines)

Surface pressure distribution by both experiments and computations is shown in Figure 13 and Figure 14 for the open and closed gap models, respectively. The agreement between measurements and computations is excellent, even in the gap region. As observed in the cavitation inception tests, the negative pressure peaks reach 1.45 and 1.33 for the open and closed gap models, respectively. Also the cavitation locations, i.e., the negative pressure peak locations, are consistent with the ones observed in the cavitation visualization.

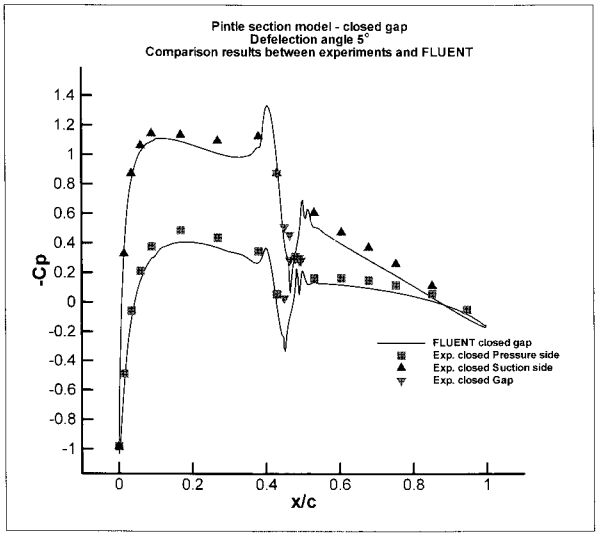

Figure 14: Surface pressure coefficient with closed gap: Experiments (symbols); Computations (lines)

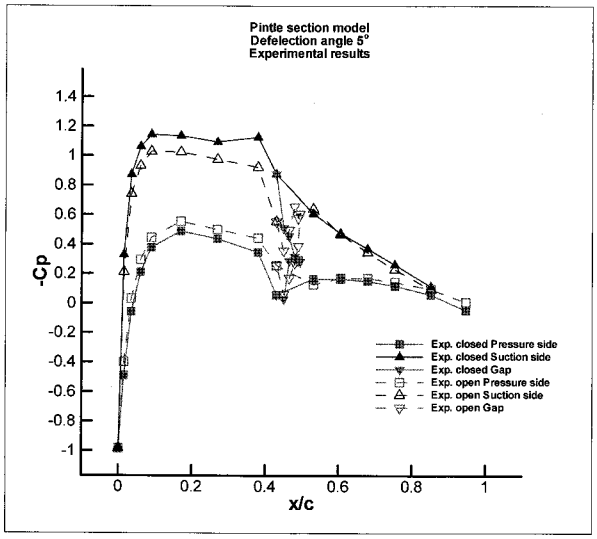

Figure 15: Pressure coefficients at open/closed gap

Finally, Figure 15 shows the comparison of surface pressure coefficients with open and closed gaps. It is clearly seen that the surface pressure difference between the suction and pressure sides of the model is larger with closed gap, which leads to the lift augmentation. Also of interest in Figure 15 is that the largest pressure difference is observed on the stationary part, especially on the suction side, which results in earlier leading edge cavitation with closed gap.

6 Conclusions

Rudder gap cavitation and effectiveness of its suppression devices are studied using experiments and computations. Incipient cavitation numbers are identified by depressurized cavitation tunnel tests and compared with computational results by solving the RANS equations. Recorded images by a video camera are analyzed to investigate the cavitation behavior. Surface pressure measurement results confirm the incipient cavitation numbers and locations. CFD solutions for surface pressure distribution are consistent with experimental results, showing good agreement. More tests with the horn section model and other deflection angles are under way and the results will be reported in the near future.

Acknowledgements

This work was supported by the Korea Research Foundation Grant (KRF-2005-005-J10203) and the Korea Science and Engineering Foundation Grant (No. ROA-2007-000-10028-0) funded by the Korean Government.

References

Boo, G.T, I.H Song and S.C Shin. 2003a. Numerical Simulation for the Rudder in order to Control the Cavitation Phenomena. Proc. International Workshop on Frontier Technology in Ship and Ocean Engineering, Seoul, Korea.

Boo, K.T., J.M. Han, I.H. Song and S.C. Shin. 2003b. Viscous Flow Analysis for the Rudder Section Using FLUENT Code. Journal of the Society of Naval Architects of Korea, **40**, **4**, 30-36. (In Korean).

Choi, J.-E. and S.-H. Chung. 2007. Characteristics of Gap Flow of a 2-Dimensional Horn-type Rudder Section. Journal of the Society of Naval Architects of Korea, **44**, **2**, 101-110. (In Korean).

Kim, S-E, and S.H Rhee. 2002. Assessment of Eight Turbulence Models for a Three-Dimensional Boundary Layer Involving Crossflow and Streamwise Vortices. AIAA Paper 2002-0852, Proc. 40th AIAA Aerospace Sciences Meeting and Exhibit, Reno, NV, USA.

Kim, S.P., J.J Park, Y.S. Kim, Y.H. Jang, Y.B. Choi and B.G. Paik. 2006. An Experimental Research on Gap Cavitation Erosion of Semi-spade Rudder. Journal of the Society of Naval Architects of Korea, **43**, **5**, 578-585. (In Korean).

Paik, B.-G., K.-Y. Kim, J.-W. Ahn, Y.-S. Kim, S.-P. Kim and J.-J. Park. 2008. Experimental study on the gap entrance profile affecting rudder gap cavitation. Ocean Engineering, **35**, 139-149.

Park, S.H, J.K. Heo and B.S. Yu. 2007. Numerical Study on Horn Rudder Section to Reduce Gap Cavitation. 10th International Symposium on Practical Design of Ships and Other Floating Structures (2007 PRADS), **2**, Houston, Texas, USA, 1255-1260.

Rhee, S.H, and H. Kim. 2006. Analysis of Rudder Cavitation in Propeller Slipstream and Development of its Suppression Devices. Proc. 2006 SNAME Maritime Technology Conference & Expo, Ft.Lauderdale, FL.

Rhee, S.H., and B. Makarov. 2005. Validation Study for Free-Surface Wave Flows Around Surface-Piercing Cylindrical Structures. Proc. 24th International Conference on Offshore Mechanics and Arctic Engineering, Halkidiki, Greece.

Rhee, S.H., B. Makarov, H. Krishnan and V. Ivanov. 2005. Assessment of Volume of Fluid Method for Free-Surface Wave Flows. Journal of Marine Science and Technology, **10**, **4**, 173-180.

Shen, Y.T., C.W., Jiang and K.D. Remmers. 1997. A Twisted Rudder for Reduced Cavitation. J. Ship Research, **41**, **4**, 260-272.

Shih, T.-H., W.W. Liou, A. Shabbir, Z., Yang and Z. Zhu. 1995. A New k-ε Eddy-Viscosity Model for High Reynolds Number Turbulent Flows - Model Development and Validation. Computers Fluids, **24**, **3**, 227-238.

Song, I.H., K.J. Paik, S.M. Ahn, J.K. Oh and J.C. Suh. 2004. Cavitation Characteristics on various 2-Dimensional Rudder with Gap. Proc. Annual Autumn Metting of the Society of Naval Architects of Korea, Sancheong, Korea, 51-56. (In Korea).